

Seeding decay of the false vacuum

Matteo Canaletti^{1,*} and Ian G. Moss^{1,†}

¹*School of Mathematics, Statistics and Physics,
Newcastle University, Newcastle Upon Tyne, NE1 7RU, UK*

(Dated: September 5, 2024)

We present a theory of false vacuum decay induced by spherical nucleation seeds. The type of seed considered has a boundary characterised by surface energy terms. The theory applies to false vacuum decay at zero and finite temperatures. Seeded nucleation may be important for enabling future false vacuum decay experiments on analogue systems using Bose Einstein Condensates (BEC). We show that our theory of seeded nucleation at finite temperature applied to a potassium BEC in two spatial dimensions agrees with numerical, real-time, simulations.

I. INTRODUCTION

First order phase transitions in continuous media are characterised by the nucleation of bubbles which grow and coalesce. A remarkable prediction of quantum field theory is that a similar process can occur in a quantum field. This is the phenomenon of false vacuum decay [1, 2]. False vacuum decay in elementary particle physics could have significant consequences. In the early universe, false vacuum decay at finite temperature [3] could play a role in the formation of matter [4] and gravitational waves [5]. The origin of the universe could even be the result of a vacuum decay event [6]. The possibility of false vacuum decay in the present day was described by Coleman as “the ultimate ecological catastrophe” [7]. (For reviews of early universe vacuum decay see e.g. [8, 9].)

Familiar phase transitions in nature, for example the one between liquid and gaseous phases of water, most often proceed with the assistance of nucleation seeds. In clouds, dust in the upper atmosphere plays a key role in the formation of water droplets (e.g. [10]). In this paper, we sketch out a general theory of nucleation near boundaries in quantum field theory, based on ideas from the thermodynamical study of liquid-vapour systems (e.g [11]).

For our discussion, a seed is any region which has a boundary with the true or false vacuum phase, but is not itself in either phase. We do not consider any energy input, as might occur in

* matteo.canaletti@gmail.com

† ian.moss@newcastle.ac.uk

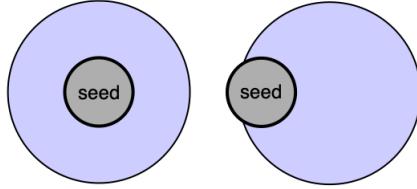


FIG. 1. Seeded bubble nucleation. In the left figure the seed is inside a bubble of true vacuum and in the right figure on the edge of the bubble.

a particle collision event. We will also restrict ourselves to spherical seeds. Surface energy contributions play an important role in the theory, and so we assume that the bubbles have sufficiently well-defined boundaries for this.

Examples of seeded nucleation in quantum field theory exist already in the literature. Nucleation seeded by black holes was introduced in Refs. [12–16]. Nucleation by quantum vortices was the examined in Ref. [17]. Bubbles can act like seeds in models with multiple false vacua, producing “barnacles” on bubble walls [18]. Enhancement of vacuum decay due to particle collisions has also been considered in the past, [19–22], although this is arguably better classed as “catalysed” rather than seeded.

Interesting questions surround the geometry of the seeded bubble nucleation event. There are two possibilities, the bubble surrounds the seed, which we call interstitial nucleation, or the bubble intersects the seed, which we call edge nucleation. We show that edge nucleation is the far more likely of the two. (This has already been seen in liquid droplet systems [23].)

An important motivation for this paper has been the recent interest in experiments on false vacuum decay in the laboratory. Bose-Einstein Condensates (BEC) are especially relevant because they can be described by a coherent quantum field. It is possible for a multi-component BEC to have regimes in which it behaves like a analogue system with a false vacuum state. The first experimental demonstration of false vacuum decay at finite temperature has been achieved in a sodium BEC [24]. Earlier theoretical proposals have shown that the effective theory in some systems can possess Lorentz invariance [25–27]. In these systems, a metastable false vacuum state exists, which is expected to decay by Coleman-type bubble nucleation [28–30]. Simulations at finite temperature indicate that the decay can be described by thermal instantons [31–33].

In future laboratory experiments, it may be useful to force bubble nucleation events in order to study how they grow and interact. This could be done by imprinting a region with the true vacuum state artificially. The alternative would be to seed bubbles, for example by depleting the density of

atoms in a small region. The seeding method has the advantage of testing some aspects of bubble nucleation theory, which the imprinting method cannot.

In the final section of this paper, we describe a numerical simulation of bubble nucleation around a seed in a potassium-39 BEC at finite temperature, based on the scheme proposed in [34]. The seed is created by creating a region of high potential, which forces the density to drop. Nucleation is enhanced, as expected, and the nucleation is always of the edge type.

II. GENERAL CONSIDERATIONS

A. Bubble nucleation

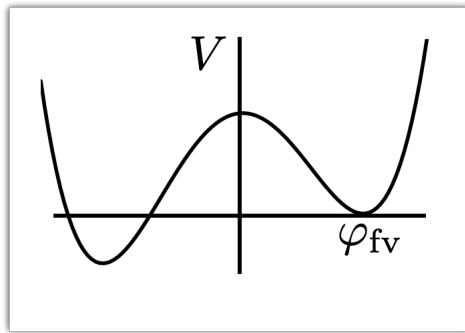


FIG. 2. The potential of an effective field theory with true and false vacua.

Bubble nucleation is a feature of false vacuum decay [1, 2] and first order phase transitions [35]. Both can be described using effective field theories. In the thermal case, the initial state is a thermal ensemble of particle excitations about the false vacuum field φ_{FV} . We follow Ref. [3] in describing this case as false vacuum decay at finite temperature. The nucleation rate of bubbles in the thermal or false vacuum state is given by a universal formula, depending on an instanton solution φ_b to the effective field equations. Instanton solutions use an imaginary time coordinate, $t = i\tau$ and their action is pure imaginary iS_E , where S_E is termed the Euclidean action. The rate of bubble nucleation Γ in a volume \mathcal{V} is [1, 2]

$$\Gamma = \mathcal{V} \left| \frac{\det' S_E''[\varphi_b]}{\det S_E''[\varphi_{FV}]} \right|^{-1/2} \left(\frac{B}{2\pi} \right)^{n/2} e^{-B}, \quad (1)$$

where the tunneling exponent is

$$B = \frac{S_E[\varphi_b] - S_E[\varphi_{FV}]}{\hbar}, \quad (2)$$

and S_E'' denotes the second functional derivative of the action. The determinant of an operator is the product of its eigenvalues, and a prime implies omitting n zero modes, each one of these corresponding to a translational degree of freedom of the instanton. In the case of thermal bubble nucleation at a first order phase transition the instantons are independent of imaginary time and the Euclidean action reduces to $S_E/\hbar = E/k_B T$, where E is the energy. (Although Planck's constant has disappeared from the exponent in the thermal case, it can still appear in the operators, and then the tunnelling rate is set by quantum, rather than classical, field theory.)

We will simplify the expression for the rate to

$$\Gamma = A_b \mathcal{V} B^{n/2} e^{-B}. \quad (3)$$

In D spatial dimensions, there are $n = D + 1$ translational symmetries in the vacuum case, and $n = D$ in the thermal case. The pre-factor A_b is constructed from the functional determinants, and depends on the parameters of the model. In a relativistic system with speed of light c , a useful approximation is that $A_b \propto R^{-D-1} c$, where R is the bubble radius, based on dimensional analysis.

Now consider what happens when the bubble nucleates around a nucleation seed, and the number density of seeds is n_s . Bubble nucleation can happen with a seed at the centre, which we call interstitial, or at the edge. In either case, the exponent B_s and the pre-factor A_s will depend on the seed geometry. In the interstitial case, assuming some limited freedom on position of the seed inside the bubble, and having $\mathcal{V} n_s$ seeds in total,

$$\Gamma_s = A_s \mathcal{V} n_s B_s^{n/2} e^{-B_s}. \quad (4)$$

In the edge case, the number of zero modes n equals the surface dimension of the seed. The zero modes will contribute a factor proportional to the surface area of the seed \mathcal{A}_s ,

$$\Gamma_s = A_s \mathcal{V} n_s \mathcal{A}_s B_s^{n/2} e^{-B_s}. \quad (5)$$

We will make an assumption that the pre-factor A_s contributes a relatively minor dependence on the seed properties.

B. Phase equilibria and instantons

The thin-wall limit is one where a bubble of a lower energy “true” phase TV is separated by a wall from the surrounding “false” phase FV , and the wall is thinner than the bubble radius R . The true phase exerts an outward pressure on the wall equal to the energy density difference ϵ

between the two phases. The size of a thermal bubble is determined by a balance between this pressure force and the force due to surface tension of the wall σ_{TF} . In three dimensions, this is expressed by Laplace’s relation for the principle radii of curvature R_1 and R_2 of the bubble wall,

$$\frac{1}{R_1} + \frac{1}{R_2} = \frac{\epsilon}{\sigma_{TF}}. \quad (6)$$

Laplace’s relation generalises to arbitrary dimension D if we use the $D - 1$ principle radii of curvature. In the fully symmetric case, the bubble radius R is therefore given by $R = (D - 1)\sigma_{TF}/\epsilon$.

When any kind of barrier is introduced, there are additional surface tension terms to take into account,

- σ_{ST} between the seed and true vacuum phase
- σ_{SF} between the seed and false vacuum phase
- σ_{TF} between true and false vacuum phases

The balance of forces at the triple boundary determines an angle of contact θ by Young’s equation (see figure 5),

$$\cos \theta = \frac{\sigma_{SF} - \sigma_{ST}}{\sigma_{TF}}. \quad (7)$$

Small angles are associated with a “wetable” surfaces, and angles close to π with “hydrophobic” surfaces.



FIG. 3. Left: Surface tensions and angle of contact θ for the true vacuum region (shaded). Right: A true vacuum bubble of volume \mathcal{V} nucleating beside a boundary, with contact area \mathcal{A}_W between the true vacuum phase and the wall.

An analogous situation exists for the instanton solutions in the theory of false vacuum decay at zero temperature. An extra dimension is added to represent imaginary time and the energy is replaced by the Euclidean action. In a Lorentz invariant theory, there is an equivalence between dynamics in D spatial dimensions and $D + 1$ Euclidean dimensions, implying that Laplace’s and young’s relations still hold. (This can also be confirmed from the Euler-Lagrange equations for the Euclidean action.) In free space, bubbles are spheres in $D + 1$ dimensions, with radii $R = D\sigma_{TF}/\epsilon$.

C. Tunnelling exponents

The bubble nucleation rate in a metastable state takes the exponential form given in Eqs. (4) and (5) with exponent B . Both vacuum and thermal tunnelling can be considered together if we introduce the speed of light c and make the following normalisations:

- σ and ϵ are normalised by $\hbar c$ in the vacuum case
- σ and ϵ are normalised by $k_B T$ in the thermal case

In addition, the bubbles in the vacuum case have structure in the imaginary time direction. We will retain the notation D as the spatial dimension, so that the bubbles exist in $D + 1$ dimensions in the vacuum case.

When walls are included, as in figure 3, the tunnelling exponent is given by the total energy (or Euclidean action) difference between the system with a bubble and the system without a bubble,

$$B = \mathcal{A}_W(\sigma_{ST} - \sigma_{SF}) + \mathcal{A}_B\sigma_{FT} - \epsilon\mathcal{V}. \quad (8)$$

Young's equation (7) can be used to simplify this expression,

$$B = (\mathcal{A}_B - \mathcal{A}_W \cos \theta) \sigma_{FT} - \epsilon\mathcal{V}. \quad (9)$$

Note that the contact angle θ is a fixed quantity and the radii of curvature will be extrema of the tunnelling exponent.

For a free spherical bubble not attached to a wall, $\mathcal{A}_W = 0$ and the radii of curvature are equal. The bubble radius R and tunnelling exponent B_b for free bubbles in D spatial dimensions are given by

$$\text{thermal case} \quad R = \frac{(D-1)\sigma_{TF}}{\epsilon}, \quad B_b = \frac{\epsilon\mathcal{V}_D R^D}{D-1}, \quad (10)$$

$$\text{vacuum case} \quad R = \frac{D\sigma_{TF}}{\epsilon}, \quad B_b = \frac{\epsilon\mathcal{V}_{D+1} R^{(D+1)}}{D}. \quad (11)$$

where \mathcal{V}_N is the volume of a unit sphere in N dimensions.

III. SPHERICAL SEEDS

The two possibilities are bubbles that surround the seed (interstitial) and bubbles that nucleate on the edge (edge). The energy of spherical liquid droplets around seeds has been investigated previously in more down to earth contexts, e.g [23].

A. Interstitial case-thermal

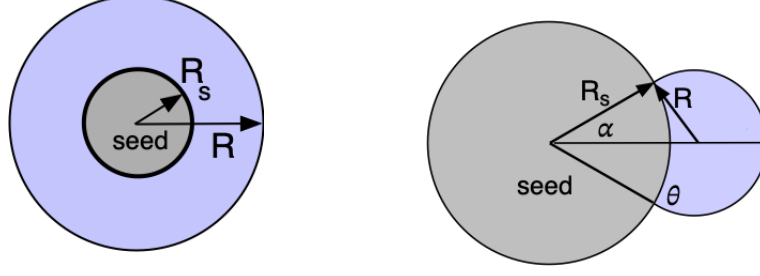


FIG. 4. A bubble with interstitial seed (left) and a bubble on the edge of the seed (right).

Consider a bubble of radius R and a seed of radius R_s . In the interstitial case, the bubble has spherical symmetry with $R = (D - 1)\sigma_{TV}/\epsilon$ from Eq. (10), and we have

$$\mathcal{V} = \mathcal{V}_D(R^D - R_s^D), \quad (12)$$

$$\mathcal{A}_B = D\mathcal{V}_D R^{D-1}, \quad (13)$$

$$\mathcal{A}_W = D\mathcal{V}_D R_s^{D-1}, \quad (14)$$

where \mathcal{V}_D is the volume inside a unit sphere in D dimensions. The exponent from Eq. (9) is

$$B = B_b \left\{ 1 - \left(\frac{R_s}{R} \right)^{D-1} D \cos \theta + (D - 1) \left(\frac{R_s}{R} \right)^D, \right\}, \quad (15)$$

where the free tunnelling exponent B_b is given in Eq.(10), and the contact angle is fixed by Young's relation $\cos \theta = (\sigma_{SF} - \sigma_{ST})/\sigma_{TF}$. The nucleation rate has a minimum with a seed radius $R_s = R \cos \theta$ when $\cos \theta > 0$, giving an enhanced nucleation rate, as shown in figure 5. When $\theta \geq \pi/2$, $B \geq B_b$ for any seed radius, and nucleation around the seed is always disfavoured.

B. Edge case-thermal

In the edge case, rotational symmetry about the axis joining the centre of the seed to the centre of the bubble implies that the radii of curvature of the bubble have the same value R , and the bubble is part of a sphere. The tunnelling exponent is given by the general formula Eq. (9), where the areas and volumes can all be obtained from elementary Euclidean geometry.

We introduce the angle α subtended by the bubble at the seed centre,

$$\tan \alpha = \frac{R \sin \theta}{R_s - R \cos \theta}. \quad (16)$$

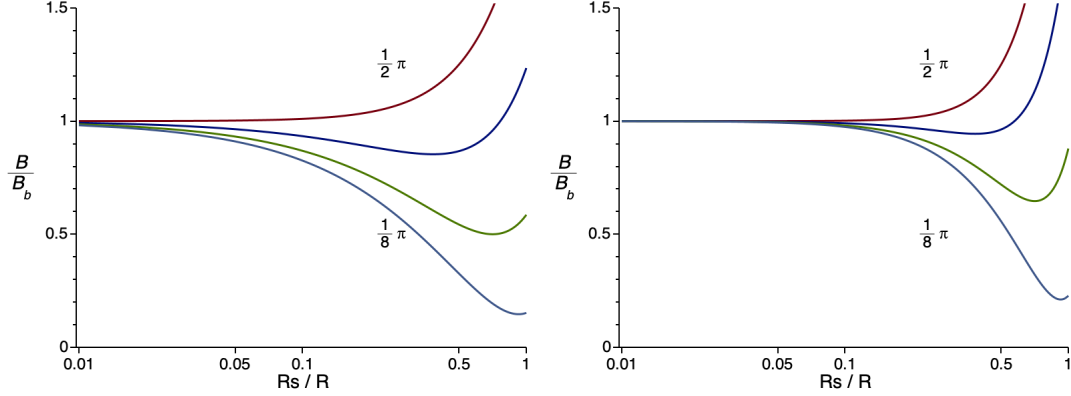


FIG. 5. The thermal tunnelling exponent B for interstitial seeds normalised by the free bubble case, as a function of the seed radius R_s divided by the bubble radius $R = (D - 1)\sigma_{TF}/\epsilon$. The curves are labeled by the angle of contact θ , which is fixed by Young's relation $\cos \theta = (\sigma_{SF} - \sigma_{ST})/\sigma_{TF}$. The left-hand plot is in two spatial dimensions, $D = 2$, and the right hand plot in three spatial dimensions, $D = 3$.

In two spatial dimensions,

$$\mathcal{A}_W = 2R_s\alpha, \quad (17)$$

$$\mathcal{A}_B = 2R(\alpha + \theta), \quad (18)$$

$$\mathcal{V} = R^2 \left[(\alpha + \theta) - \frac{1}{2} \sin 2(\alpha + \theta) \right] - R_s^2 \left[\alpha - \frac{1}{2} \sin 2\alpha \right]. \quad (19)$$

The tunnelling exponent is found after eliminating α . For example, with a contact angle $\theta = \pi/2$, the tunnelling exponent becomes

$$B = B_b \left\{ \left(\frac{1}{2} + \frac{1}{\pi} \arctan \frac{R}{R_s} \right) + \frac{1}{\pi} \frac{R_s^2}{R^2} \arctan \frac{R}{R_s} - \frac{1}{\pi} \frac{R_s}{R} \right\}, \quad (20)$$

where $B_b = \epsilon\pi R^2$. In this case, the exponent runs from B_b at $R_s = 0$ down to $B_b/2$ as $R_s \rightarrow \infty$. Seeded nucleation is therefore favoured at $\theta = \pi/2$, unlike in the interstitial case.

For three spatial dimensions,

$$\mathcal{A}_W = 2\pi R_s^2 [1 - \cos \alpha], \quad (21)$$

$$\mathcal{A}_B = 2\pi R^2 [1 - \cos(\alpha + \theta)], \quad (22)$$

$$\mathcal{V} = \frac{\pi}{3} R^3 [2 - 3 \cos(\alpha + \theta) + \cos^3(\alpha + \theta)] - \frac{\pi}{3} R_s^3 [2 - 3 \cos \alpha + \cos^3 \alpha]. \quad (23)$$

The tunnelling exponents in two and three spatial dimensions are shown in figure 6, for a range of contact angles. The tunnelling exponent is always smaller on the edge of a nucleation seed. The effect is most pronounced when the seed is larger than the bubble radius and the contact angle is small, and is likely to dominate over changes to the pre-factor discussed earlier. When the

contact angle $\theta = \pi/2$, and the seed radius is large, the tunnelling exponent is exactly half of the bulk case, corresponding to having half an instanton.

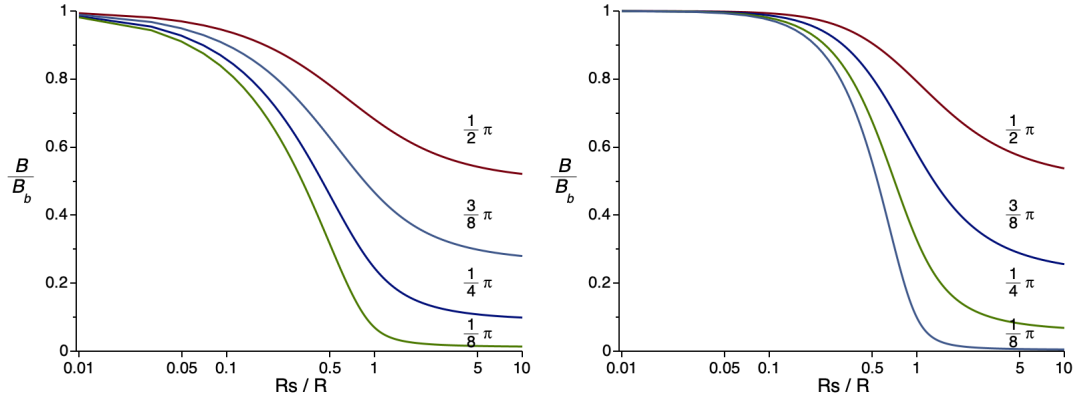


FIG. 6. The thermal tunnelling exponent B for the edge nucleation normalised by the free bubble case, as a function of the seed radius R_s divided by the bubble radius $R = (D-1)\sigma_{TF}/\epsilon$. The curves are labeled by the angle of contact θ , which is fixed by the surface tensions. The left-hand plot is in two spatial dimensions, $D = 2$, and the right hand plot in three spatial dimensions, $D = 3$.

C. Interstitial case-vacuum

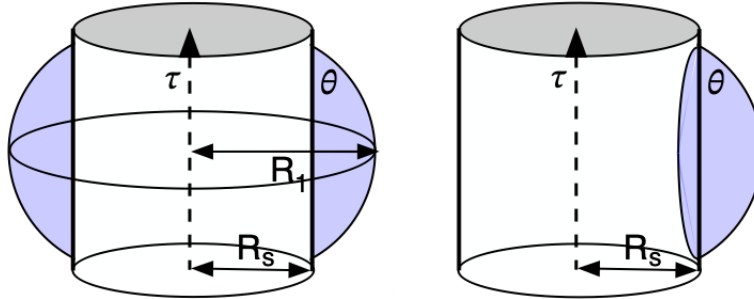


FIG. 7. In the vacuum case, the seed extends into the imaginary time direction. The bubble wall meets the seed with angle θ , but the bubble radii of curvature are no longer equal. Left: interstitial case. Right: Edge case.

We restrict attention to Lorentz invariant systems with velocity of light c . The seed is a cylinder extended in the imaginary time direction. The bubble wall meets the seed along the imaginary time direction, as shown in figure 7. The bubble wall is no longer spherical, but in the interstitial case it has cylindrical symmetry with surface $r(\tau)$ in cylindrical coordinates. Imaginary time ranges from $-\tau_s \leq \tau \leq \tau_s$, where $r(\tau_s) = R_s$.

The bubble surface is a stationary point of the exponent B given by Eq. (9), where the areas and volumes are given by

$$\mathcal{A}_W = 2D\mathcal{V}_D R_s^{D-1} \int_0^{\tau_s} c d\tau, \quad (24)$$

$$\mathcal{A}_B = 2D\mathcal{V}_D \int_0^{\tau_s} c d\tau r^{D-1} (1 + r'^2/c^2), \quad (25)$$

$$\mathcal{V} = 2\mathcal{V}_D \int_0^{\tau_s} c d\tau (r^D - R_s^D). \quad (26)$$

The Euler-Lagrange equations for the bubble surface have a first integral,

$$E = r^D - \frac{r^{D-1}}{(1 + r'^2/c^2)^{1/2}} R. \quad (27)$$

The boundary condition $r' = c \tan \theta$ at the seed and $r' = 0$ at the plane of symmetry $\tau = 0$ imply

$$E = R_s^D - R R_s^{D-1} \cos \theta = R_1^D - R R_1^{D-1}. \quad (28)$$

Substituting the equation for the bubble wall (27) into B gives

$$B = 2\mathcal{V}_D \epsilon \int_{R_s}^{R_1} dr [r^{2D-2} R^2 - (E - r^D)^2]^{1/2}, \quad (29)$$

where E and R_1 are determined by Eq. (28) as functions of R_s and θ . The result of evaluating the integral is shown for two and three spatial dimensions in figure 8. The tunnelling rate is considerably enhanced for small contact angles. Unlike the thermal case, in the vacuum bubble case the seed can be larger than the mean curvature radius R .

D. Edge case-vacuum

For vacuum tunnelling in the edge case, the bubble sits on the edge of a cylinder, as in figure 7. The energy of bubbles with this geometry has been investigated in three spatial dimensions [36]. Unfortunately, these results were presented for fixed volume instead of fixed ‘‘pressure’’. Finding the bubble shape in general is a complex numerical problem which we will not pursue further here. However, we can obtain approximate results in the large seed radius limit, by adapting formulae from Ref. [36] (see appendix A).

In two spatial dimensions,

$$\frac{B}{B_b} = \frac{1}{2} \left(1 - \cos \theta - \frac{1}{2} \cos \theta \sin^2 \theta \right) + \frac{3}{16} \frac{R}{R_s} \sin^4 \theta + O(R^2/R_s^2). \quad (30)$$

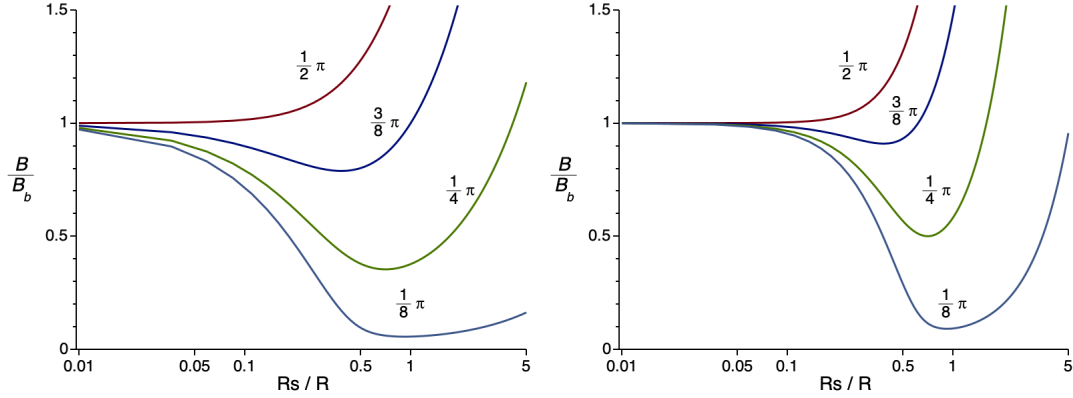


FIG. 8. The vacuum tunnelling exponent B for an interstitial seed normalised by the free bubble case, as a function of the seed radius R_s normalised by the mean curvature radius $R = D\sigma_{TF}/\epsilon$. The curves are labeled by the angle of contact θ , which is fixed by the surface tensions. The left-hand plot is in two spatial dimensions, $D = 2$, and the right hand plot in three spatial dimensions, $D = 3$.

In three spatial dimensions,

$$\frac{B}{B_b} = \frac{1}{\pi} \left(\theta - \sin \theta \cos \theta - \frac{2}{3} \cos \theta \sin^3 \theta \right) + \frac{4}{5\pi} \frac{R}{R_s} \sin^5 \theta + O(R^2/R_s^2). \quad (31)$$

A useful check is that the instanton should become hemi-spherical in the limit $\theta = \pi/2$ and $R_s \rightarrow \infty$. Bubbles in the bulk are spherical, and we expect $B/B_b = 1/2$, as is the case from the formulae.

The vacuum tunnelling exponents are plotted in figure 9. Compared to the interstitial case in figure 8, these are much smaller. Therefore, at least in this regime, vacuum bubble nucleation is predominantly seeded at the edge.

IV. ANALOGUE SYSTEMS

The analogue system we consider here is similar to the one described in Ref [34]. It is based on potassium atoms occupying two hyperfine levels condensed in a two-dimensional atom trap. We regard the atoms in the two levels as two separate components of the BEC. Atomic collisions between atoms in the same level, or different levels, are described by three parameters g_{11} , g_{22} and g_{12} . In addition, a modulated microwave field provides mixing between the atoms in each level, described by a Rabi frequency Ω and a dimensionless parameter λ . The scattering parameters g_{ij} determine the relative number density of the two components in the ground state of the system, n_1 and n_2 . Important physical parameters are the frequency scale $\omega_m = (g_{11} + g_{22} - 2g_{12})n/\hbar$ and healing length $\xi_m = (\hbar/m\omega_m)^{1/2}$, where $n = n_1 + n_2$ is the total density.

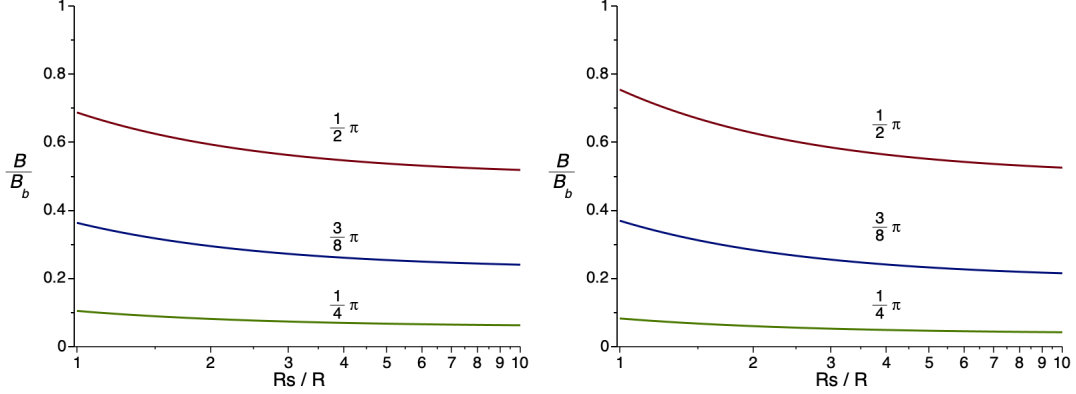


FIG. 9. The vacuum tunnelling exponent B for edge nucleation normalised by the free bubble case, as a function of the seed radius R_s normalised by the mean curvature radius $R = D\sigma_{TF}/\epsilon$. The curves are labelled by the contact angle θ . The left-hand plot is in two spatial dimensions, $D = 2$ and the right hand plot in three spatial dimensions, $D = 3$.

An additional trapping potential $V_T(x, y)$ is used as a nucleation seed. Inside the seed, the potential drives the density to zero. There is a narrow transition region at the edge of the seed, which we can arrange to have a width approximately equal to ξ_m . The density outside the seed has a constant value n in the initial state.

In [34], it was shown that the system can be described by an effective theory for a single scalar field related to the relative phase φ of the two components. The canonically normalised field $\phi = v\varphi$, where

$$v^2 = n_1 n_2 \xi_m^2 \hbar \omega_m / n. \quad (32)$$

The field equation has Klein-Gordon form,

$$c_\varphi^{-2} \ddot{\phi} - \nabla^2 \phi + \frac{dV}{d\phi} = 0, \quad (33)$$

where the sound speed $c_\varphi = \xi_m \omega_m (n_1 n_2)^{1/2} \sqrt{2}/n$ and the potential

$$V(\phi) = \hbar \Omega \sqrt{n_1 n_2} \left(-\cos \frac{\phi}{v} + \frac{1}{2} (\lambda^2 - 1) \sin^2 \frac{\phi}{v} \right). \quad (34)$$

When $\lambda^2 > 1$, the potential has a local minimum, or false vacuum, at $\phi = v\pi$ and a global minimum, or true vacuum, at $\phi = 0$. The energy density difference between the vacua is $\epsilon = 2\hbar\Omega\sqrt{n_1 n_2}$.

For the finite temperature simulations, we solve the Projected Stochastic Gross-Pitaevski Equation (SPGPE) for the condensate fields ψ_i [37]. The SPGPE is

$$i\hbar \frac{\partial \psi_i}{\partial t} = \mathcal{P} \left\{ (1 + i\gamma) \frac{\partial H}{\partial \psi_i} + \eta_i \right\}, \quad (35)$$

where H is the Hamiltonian, $i\gamma$ is a dissipation term and η_m is a Gaussian stochastic noise term with statistics

$$\langle \eta_i(\mathbf{r}, t) \eta_j^\dagger(\mathbf{r}', t') \rangle = \frac{2\gamma k_B T}{\hbar \omega_m n} \delta_{ij} \delta(\mathbf{r} - \mathbf{r}') \delta(t - t'). \quad (36)$$

The equation is solved in a two dimensional periodic box with the trapping potential seed at the centre. Averages over many runs are used to find the bubble nucleation rate for a range of seed sizes.

The system is initialised in the false vacuum state. This is achieved by equilibrating in the true vacuum state and changing the sign of the Rabi frequency Ω with a piecewise linear ramp. This switches the true and false vacua. Bubble nucleation times are evaluated relative to the end of the ramp. The nucleation rate is extracted by fitting the nucleation times to a Poisson distribution. (A small time offset parameter is included to allow for the bubble nucleation detection algorithm and nucleation during the ramp.)

Bubble nucleation in a typical run is shown in figure 10. The pictures show the cosine of ϕ/v , where ϕ is the degree of freedom of the effective field theory. In the false vacuum phase $\cos(\phi/v) = -1$, and in the true vacuum phase $\cos(\phi/v) = 1$. The field ϕ is not defined inside the seed where the atomic density vanishes. Bubbles of true vacuum phase nucleate, as expected, on the edge of the seed, with contact angle is around $\pi/2$. They grow at the sound speed for the BEC.

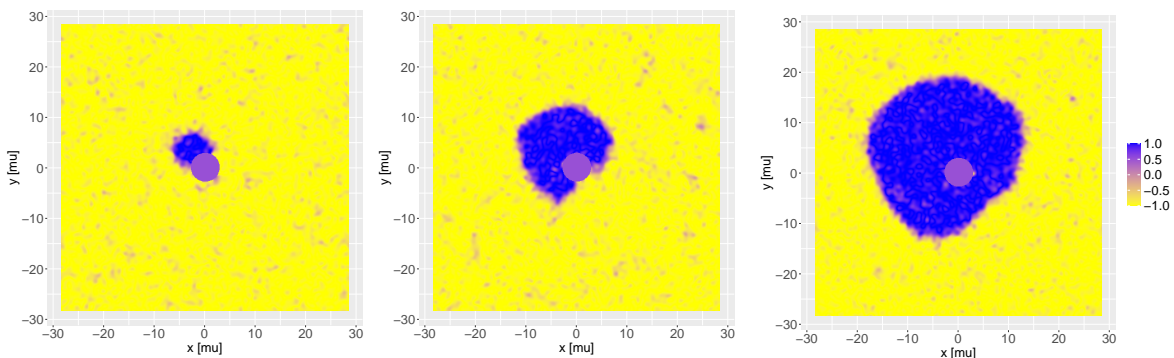


FIG. 10. Simulated thermal bubble nucleation around a circular seed for a two dimensional BEC. The plot shows the cosine of the relative phase of the two components. The seed is the grey circle in the centre. Snapshots are taken at 28ms, 29ms and 30ms. This 39K model has 200 atoms per square micron, temperature 160nK, healing length $\xi_m = 0.142 \mu\text{m}$, frequency $\omega_m = 14.0 \times 2\pi \text{ kHz}$ and Rabi frequency $\Omega = 100 \times 2\pi \text{ Hz}$.

For comparison with the theory presented earlier, we fit the seeded nucleation rate Γ_s to the formula

$$\Gamma_s = A_s R_s B_s^{1/2} e^{-B_s}, \quad (37)$$

where $B_s \equiv B_s(B_b, R, R_s)$ is given by Eq. (20). For small seeds, the bulk nucleation rate Γ_b can exceed the seeded rate. The bulk nucleation rate depends on the size L of the periodic box,

$$\Gamma_b = A_b L^2 B_b e^{-B_b}. \quad (38)$$

The total nucleation rate $\Gamma = \Gamma_s + \Gamma_b$ can be fit with four parameters A_s , A_b , B_b and R . (In practice, we reduced to three parameters by fixing the $R_s = 0$ point). The rates are shown in figure 11, assuming the contact angle of $\theta = \pi/2$ as predicted by theory (see appendix B), and seen in pictures such as figure 10. The results suggest that the theory is a good description of seeded nucleation, even though the theory uses a thin-wall approximation and the actual bubble walls are quite broad.

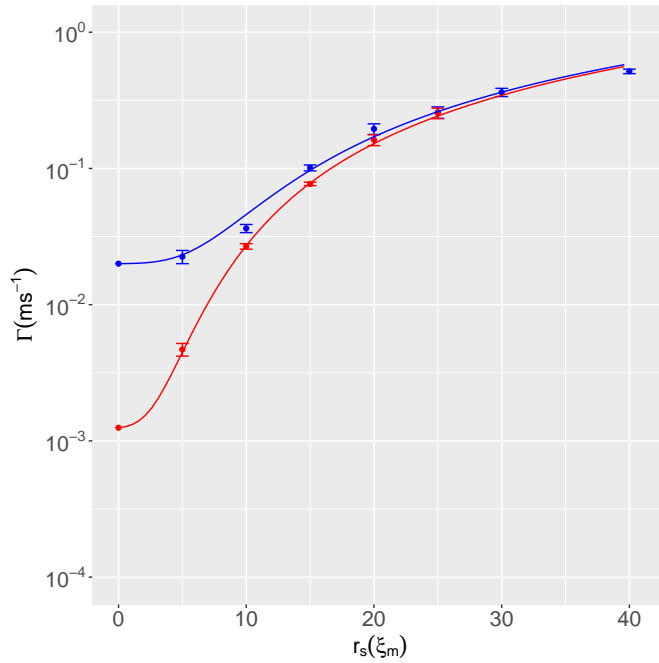


FIG. 11. Bubble nucleation rate Γ plotted as a function of the seed radius R_s in healing length units. The upper curve is for a periodic box of side $L = 400\xi_m$ and the lower curve $L = 200\xi_m$. The curves are a fit to the data using the theory described in the text. The fitting parameters are bubble radius $R = 9.2\xi_m$ and free nucleation exponent $B_b = 14.7$. The contact angle $\theta = \pi/2$.

V. CONCLUSION

We have presented fairly comprehensive results for tunnelling exponents in false vacuum decay at zero and nonzero temperature around a spherical nucleation seed. We have looked at both two and three spatial dimensions. Whilst the three dimensional case is the one applicable to the universe, two dimensions have applications to analogue false vacuum decay experiments. In this context, we have compared the thermal nucleation rates to a numerical simulation of the time evolution of a Bose Einstein condensate. There is good agreement between the instanton and real-time approaches, even though the bubbles in this system don't have the thin walls used in the instanton theory. It would be fascinating to compare the instanton theory to the vacuum nucleation in a real experiment.

The form that nucleation seeds might take in an early universe application is an open question. Our results do not apply directly to some of the proposals on nucleation that have been put forward. However, it is tempting to speculate. Black hole seeding of bubble nucleation has only been looked at with spherical symmetry so far [12, 13]. Our results have a definite preference for bubbles appearing on the edge of seed, which is not a spherically symmetric configuration.

In the case of proton or heavy ion collisions, the initial collision region is likely to be pancake shaped due to the Lorentz contraction of the particles. In the right conditions, the energy can redistribute itself into a more spherical region, with fluid-like properties. This is not so dissimilar to the seeds we have considered here, and it may be possible to define surface energy or actions to apply the general theory.

DATA AVAILABILITY STATEMENT

Data supporting this publication are openly available under a Creative Commons CC-BY-4.0 License in [38]

ACKNOWLEDGMENTS

The authors are grateful for discussion with Tom Billam, Kate Brown and Alex Jenkins. This work is supported by the UK Science and Technology Facilities Council [grants ST/T00584X/1 and ST/W006162/1].

Appendix A: Bubbles on cylinders

This appendix gives the mapping of functions from the liquid droplet problem in Ref. [36] to the vacuum bubble nucleating on the edge of a seed in two spatial dimensions. The relevant functions defined in Ref. [36] are

$$A_0(r) = \frac{1}{4}r^2, \quad (\text{A1})$$

$$C_0(\theta) = -\frac{1}{4}\sin^2\theta. \quad (\text{A2})$$

In addition, the droplet problem parameterises changes in R by a constant k . We have fixed R , so that $k = 0$ in our application. Quoting Eqs (24), (38) and (39)¹ from [36], and putting in the correct scaling by the mean curvature radius R ,

$$\mathcal{V} = \frac{\pi}{3}R^3 \left(1 - \cos\theta - \frac{1}{2}\cos\theta\sin^2\theta \right) + \frac{3\pi}{8}R^4R_s^{-1}\sin^4\theta + O(R^5R_s^{-2}), \quad (\text{A3})$$

$$\mathcal{A}_B = 2\pi R^2(1 - \cos\theta) + \pi R^3R_s^{-1}\sin^2\theta + O(R^5R_s^{-2}), \quad (\text{A4})$$

$$\mathcal{A}_W = \pi R^2\sin^2\theta + \pi R^3R_s^{-1}\cos\theta\sin^2\theta + O(R^5R_s^{-2}). \quad (\text{A5})$$

These can be used in Eq. (9) with $R = 2\sigma_{TF}/\epsilon$ to eliminate σ_{TF} ,

$$B = \frac{\pi}{3}\epsilon R^3 \left(1 - \cos\theta - \frac{1}{2}\cos\theta\sin^2\theta \right) + \frac{\pi}{8}\epsilon R^4R_s^{-1}\sin^4\theta + O(R^5R_s^{-2}). \quad (\text{A6})$$

For comparison, the bulk tunnelling exponent from Eq. (11) is $B_b = 2\pi\epsilon R^3/3$.

Extending the result to three spatial dimensions simply involves replacing the area measure $2\pi r dr$ by $4\pi r^2 dr$. The volumes and areas become

$$\mathcal{V} = \frac{\pi}{2}R^4 \left(\theta - \sin\theta\cos\theta - \frac{2}{3}\cos\theta\sin^3\theta \right) + \frac{8\pi}{15}R^5R_s^{-1}\sin^5\theta + O(R^6R_s^{-2}), \quad (\text{A7})$$

$$\mathcal{A}_B = 2\pi R^3(\theta - \cos\theta\sin\theta) + 2\pi R^4R_s^{-1}\sin^3\theta + O(R^6R_s^{-2}), \quad (\text{A8})$$

$$\mathcal{A}_W = \frac{4\pi}{3}R^3\sin^3\theta + 2\pi R^4R_s^{-1}\cos\theta\sin^3\theta + O(R^6R_s^{-2}). \quad (\text{A9})$$

Using Eq. (9) with $R = 3\sigma_{TF}/\epsilon$ gives

$$B = \frac{\pi}{6}\epsilon R^4 \left(\theta - \sin\theta\cos\theta - \frac{2}{3}\cos\theta\sin^3\theta \right) + \frac{2\pi}{15}\epsilon R^5R_s^{-1}\sin^5\theta + O(R^6R_s^{-2}). \quad (\text{A10})$$

The bulk tunnelling exponent is $B_b = \pi^2\epsilon R^4/6$.

¹ In Eq. (39) of Ref. [36], $\cos\alpha$ should read $\cos\alpha\sin\alpha$.

Appendix B: Contact angle for the analogue system

The two state system in two dimensions with condensate field $\psi = \{\psi_1, \psi_2\}$, and trapping potential V_T , has Hamiltonian

$$H = \int \left\{ -\frac{\hbar^2}{2m} \psi^\dagger \nabla^2 \psi + \frac{1}{2} \sum_{i,j} g_{ij} |\psi_i|^2 |\psi_j|^2 + (V_T - \mu) \psi^\dagger \psi - \frac{\hbar\Omega}{2} \psi^\dagger \sigma_x \psi + \frac{\hbar\Omega}{2} g' (\psi^\dagger \sigma_y \psi)^2 \right\} dx dy, \quad (\text{B1})$$

where $g' = \lambda^2/4\sqrt{n_1 n_2}$, the σ are Pauli matrices, and other parameters were defined in the main text. We use a Bloch sphere representation for the fields,

$$\psi_1 = \sqrt{n} \cos \frac{\theta}{2} e^{i(\phi+\varphi)/2}, \quad (\text{B2})$$

$$\psi_2 = \sqrt{n} \sin \frac{\theta}{2} e^{i(\phi-\varphi)/2}. \quad (\text{B3})$$

In Ref. [34], it was shown that the dynamics of bubble nucleation can be recovered from an effective theory using the relative phase φ with the potential (34).

To find the surface tension at the wall we consider a plane wall along the y axis, with number density $n \equiv n(x)$, and calculate the energy per unit length in the y direction. (The equations for the angular variables imply that they remain constant.) The Hamiltonian per unit length \mathcal{H} becomes

$$\mathcal{H} = \int_0^\infty \left\{ \frac{\hbar^2}{2m} (\nabla \sqrt{n})^2 + \frac{1}{2} \hat{g} n^2 + (V_T - \mu) n \pm \frac{\hbar}{2} \Omega n \sin \theta \right\} dx, \quad (\text{B4})$$

with upper and lower signs for the false and true vacuum respectively, and $\hat{g} = n \det g_{ij}/(4\hbar\omega_m)$. Variation of the Hamiltonian enables us to eliminate the chemical potential in favour of the constant vacuum density \bar{n} at $V_T = 0$,

$$\mathcal{H} = \int_0^\infty \left\{ \frac{\hbar^2}{2m} (\nabla \sqrt{n})^2 + \frac{1}{2} \hat{g} n(n - 2\bar{n}) + V_T n \right\} dx. \quad (\text{B5})$$

Note that the Rabi frequency dependence is now in \bar{n} , and there are two possible choices $\bar{n} = \bar{n}_{TV}$ and $\bar{n} = \bar{n}_{FV}$ that differ by $\bar{n}_{TV} - \bar{n}_{FV} = \hbar\Omega/\hat{g}$. For the surface tension at the wall, we have to subtract the constant density term,

$$\sigma = \mathcal{H}(n) - \mathcal{H}(\bar{n}) = \int_0^\infty \left\{ \frac{\hbar^2}{2m} (\nabla \sqrt{n})^2 + \frac{1}{2} \hat{g} (n - \bar{n})^2 + V_T (n - \bar{n}) \right\} dx. \quad (\text{B6})$$

From this, we get the field equation for n ,

$$\frac{\hbar^2}{2m} n^{-1/2} \nabla^2 n^{1/2} = \hat{g}(n - \bar{n}) + V_T. \quad (\text{B7})$$

The simplest case for a step, $V_T = 0$ for $x > 0$, has $n = \bar{n} \tanh^2(x/\xi)$ where the healing length $\xi = \hbar/(2m\hat{g}\bar{n})^{1/2}$. The integral gives

$$\sigma = \frac{2}{3}\hat{g}\xi\bar{n}^2. \quad (\text{B8})$$

However, the relevant quantity for calculating the contact angle θ is the difference $\sigma_{SF} - \sigma_{ST}$. We replace \bar{n} by the value in the respective vacua, \bar{n}_{FV} or \bar{n}_{TV} ,

$$\sigma_{SF} - \sigma_{ST} = \frac{2}{3}\hat{g}\xi_{FV}\bar{n}_{FV}^2 - \frac{2}{3}\hat{g}\xi_{TV}\bar{n}_{TV}^2 \approx -\xi_{FV}\bar{n}_{FV}\hbar\Omega, \quad (\text{B9})$$

where we have used $n_{TV} - n_{FV} = \hbar\Omega/\hat{g}$.

For the bubble wall, σ_{TF} , the thin wall approximation suggests a value determined by the integral of $[V(\phi) - V(\phi_{FV})]^{1/2}$, which results in $\sigma_{TF} = O(\Omega/\omega_m)^{1/2}$. Alternatively, the numerical tunnelling exponents for thick wall bubbles from Ref. [39] imply $B_b = O(\Omega/\omega_m)$. If we match this to the thin wall result (10), we obtain $\sigma_{TF} = O(\Omega/\omega_m)^0$. In either case, we deduce from Young's equation (7) that $\cos\theta \approx 0$ for small Ω , and $\theta \approx \pi/2$.

-
- [1] Sidney R. Coleman, “The Fate of the False Vacuum. 1. Semiclassical Theory,” *Phys. Rev.* **D15**, 2929–2936 (1977), [Erratum: *Phys. Rev.*D16,1248(1977)].
- [2] Curtis G. Callan and Sidney R. Coleman, “The Fate of the False Vacuum. 2. First Quantum Corrections,” *Phys. Rev.* **D16**, 1762–1768 (1977).
- [3] A. Linde, “Decay of the false vacuum at finite temperature,” *Nuclear Physics B* **223**, 544 (1983).
- [4] M.E. Shaposhnikov, “Baryon asymmetry of the universe in standard electroweak theory,” *Nuclear Physics B* **287**, 757–775 (1987).
- [5] C. J. Hogan, “Gravitational radiation from cosmological phase transitions,” *Monthly Notices of the Royal Astronomical Society* **218**, 629–636 (1986), <https://academic.oup.com/mnras/article-pdf/218/4/629/3299141/mnras218-0629.pdf>.
- [6] Alexander Vilenkin, “Creation of Universes from Nothing,” *Phys. Lett. B* **117**, 25–28 (1982).
- [7] Sidney R. Coleman and Frank De Luccia, “Gravitational Effects on and of Vacuum Decay,” *Phys. Rev. D* **21**, 3305 (1980).
- [8] Anupam Mazumdar and Graham White, “Review of cosmic phase transitions: their significance and experimental signatures,” *Rept. Prog. Phys.* **82**, 076901 (2019), [arXiv:1811.01948 \[hep-ph\]](https://arxiv.org/abs/1811.01948).
- [9] Mark Hindmarsh, Marvin Lüben, Johannes Lumma, and Martin Pauly, “Phase transitions in the early universe,” *SciPost Phys. Lect. Notes* , 24 (2021).
- [10] Steven J. Ghan, Hayder Abdul-Razzak, Athanasios Nenes, Yi Ming, Xiaohong Liu, Mikhail Ovchinnikov, Ben Shipway, Nicholas Meskhidze, Jun Xu, and Xiangjun Shi, “Droplet

- nucleation: Physically-based parameterizations and comparative evaluation,” *Journal of Advances in Modeling Earth Systems* **3** (2011), <https://doi.org/10.1029/2011MS000074>, <https://agupubs.onlinelibrary.wiley.com/doi/pdf/10.1029/2011MS000074>.
- [11] Mirko Gallo, Francesco Magaletti, and Carlo Massimo Casciola, “Heterogeneous bubble nucleation dynamics,” *Journal of Fluid Mechanics* **906**, A20 (2021).
- [12] I. G. Moss, “Black-hole bubbles,” *Phys. Rev. D* **32**, 1333–1344 (1985).
- [13] Ruth Gregory, Ian G. Moss, and Benjamin Withers, “Black holes as bubble nucleation sites,” *Journal of High Energy Physics* **2014** (2014), 10.1007/jhep03(2014)081.
- [14] Philipp Burda, Ruth Gregory, and Ian G. Moss, “Gravity and the stability of the higgs vacuum,” *Physical Review Letters* **115** (2015), 10.1103/physrevlett.115.071303.
- [15] Philipp Burda, Ruth Gregory, and Ian G. Moss, “Vacuum metastability with black holes,” *Journal of High Energy Physics* **2015** (2015), 10.1007/jhep08(2015)114.
- [16] Philipp Burda, Ruth Gregory, and Ian G. Moss, “The fate of the higgs vacuum,” *Journal of High Energy Physics* **2016** (2016), 10.1007/jhep06(2016)025.
- [17] Thomas P. Billam, Ruth Gregory, Florent Michel, and Ian G. Moss, “Simulating seeded vacuum decay in a cold atom system,” *Phys. Rev. D* **100**, 065016 (2019), [arXiv:1811.09169 \[hep-th\]](https://arxiv.org/abs/1811.09169).
- [18] Bartłomiej Czech, “A novel channel for vacuum decay,” *Physics Letters B* **713**, 331–334 (2012).
- [19] Ian K. Affleck and Frank De Luccia, “Induced vacuum decay,” *Phys. Rev. D* **20**, 3168–3178 (1979).
- [20] K. B. Selivanov and M. B. Voloshin, “Destruction of false vacuum by massive particles,” *JETP Lett.* **42**, 422 (1985).
- [21] John R. Ellis, Andrei D. Linde, and Marc Sher, “Vacuum stability, wormholes, cosmic rays and the cosmological bounds on $m(t)$ and $m(H)$,” *Phys. Lett. B* **252**, 203–211 (1990).
- [22] Kari Enqvist and John McDonald, “Can cosmic ray catalysed vacuum decay dominate over tunneling?” *Nucl. Phys. B* **513**, 661–678 (1998), [arXiv:hep-ph/9704431](https://arxiv.org/abs/hep-ph/9704431).
- [23] H. B. Eral, G. Manukyan, and J. M. Oh, “Wetting of a drop on a sphere,” *Langmuir* **27**, 5340–5346 (2011), pMID: 21466229, <https://doi.org/10.1021/la104628q>.
- [24] Alessandro Zenesini, Anna Berti, Riccardo Cominotti, Chiara Rogora, Ian G. Moss, Thomas P. Billam, Iacopo Carusotto, Giacomo Lamporesi, Alessio Recati, and Gabriele Ferrari, “False vacuum decay via bubble formation in ferromagnetic superfluids,” *Nature Phys.* **20**, 558–563 (2024), [arXiv:2305.05225 \[hep-ph\]](https://arxiv.org/abs/2305.05225).
- [25] O. Fialko, B. Opanchuk, A. I. Sidorov, P. D. Drummond, and J. Brand, “Fate of the false vacuum: Towards realization with ultra-cold atoms,” *EPL (Europhysics Letters)* **110**, 56001 (2015), [arXiv:1408.1163 \[cond-mat.quant-gas\]](https://arxiv.org/abs/1408.1163).
- [26] O. Fialko, B. Opanchuk, A. I. Sidorov, P. D. Drummond, and J. Brand, “The universe on a table top: engineering quantum decay of a relativistic scalar field from a metastable vacuum,” *Journal of Physics B Atomic Molecular Physics* **50**, 024003 (2017), [arXiv:1607.01460 \[cond-mat.quant-gas\]](https://arxiv.org/abs/1607.01460).
- [27] Thomas P. Billam, Kate Brown, and Ian G. Moss, “Bubble nucleation in a cold spin 1 gas,” *New J.*

- Phys.* **25**, 043028 (2023), [arXiv:2212.03621 \[cond-mat.quant-gas\]](#).
- [28] Jonathan Braden, Matthew C. Johnson, Hiranya V. Peiris, Andrew Pontzen, and Silke Weinfurter, “New Semiclassical Picture of Vacuum Decay,” *Phys. Rev. Lett.* **123**, 031601 (2019), [arXiv:1806.06069 \[hep-th\]](#).
- [29] Thomas P. Billam, Ruth Gregory, Florent Michel, and Ian G. Moss, “Simulating seeded vacuum decay in a cold atom system,” *Phys. Rev. D* **100**, 065016 (2019), [arXiv:1811.09169 \[hep-th\]](#).
- [30] Alexander C. Jenkins, Jonathan Braden, Hiranya V. Peiris, Andrew Pontzen, Matthew C. Johnson, and Silke Weinfurter, “Analog vacuum decay from vacuum initial conditions,” *Phys. Rev. D* **109**, 023506 (2024), [arXiv:2307.02549 \[cond-mat.quant-gas\]](#).
- [31] Thomas P. Billam, Kate Brown, and Ian G. Moss, “Simulating cosmological supercooling with a cold atom system,” *Phys. Rev. A* **102**, 043324 (2020), [arXiv:2006.09820 \[cond-mat.quant-gas\]](#).
- [32] Thomas P. Billam, Kate Brown, Andrew J. Groszek, and Ian G. Moss, “Simulating cosmological supercooling with a cold atom system. II. Thermal damping and parametric instability,” *Phys. Rev. A* **104**, 053309 (2021).
- [33] Dalila Pirvu, Matthew C. Johnson, and Sergey Sibiryakov, “Bubble velocities and oscillon precursors in first order phase transitions,” (2023), [arXiv:2312.13364 \[hep-th\]](#).
- [34] Alexander C. Jenkins, Ian G. Moss, Thomas P. Billam, Zoran Hadzibabic, Hiranya V. Peiris, and Andrew Pontzen, “Generalized cold-atom simulators for vacuum decay,” (2023), [arXiv:2311.02156 \[cond-mat.quant-gas\]](#).
- [35] J. S. Langer, “Statistical theory of the decay of metastable states,” *Annals Phys.* **54**, 258–275 (1969).
- [36] Majid Soleimani, Reghan J. Hill, and Theo G. M. van de Ven, “Bubbles and drops on curved surfaces,” *Langmuir* **29**, 14168–14177 (2013), <https://doi.org/10.1021/la403088r>.
- [37] Ashton S. Bradley and P. Blair Blakie, “Stochastic projected gross-pitaevskii equation for spinor and multicomponent condensates,” *Phys. Rev. A* **90**, 023631 (2014), [arXiv:1406.2029 \[cond-mat.quant-gas\]](#).
- [38] Matteo Canaletti and Ian G Moss, “Data supporting publication: Seeding decay of the false vacuum,” [10.25405/data.ncl.26797480](https://doi.org/10.25405/data.ncl.26797480).
- [39] Mario Gutierrez Abed and Ian G. Moss, “Bubble nucleation at zero and nonzero temperatures,” *Phys. Rev. D* **107**, 076027 (2023), [arXiv:2006.06289 \[hep-th\]](#).